Concealed weapons detection system using uncooled, pulsed, imaging arrays of millimeter-wave bolometers[*]

E. N. Grossman[**a], S. Nolen, N. G. Paulter, C. D. Reintsema
[a]Electromagnetic Technology Division, National Institute of Standards and Technology, Boulder, CO
[b] Electricity Division, National Institute of Standards and Technology, Gaithersburg, MD

ABSTRACT

We describe a system for detection of concealed weapons based on imaging the millimeter-wave reflectance contrast between the weapon and the human body. An architecture based upon pulsed illumination and gated integration has a large advantage in sensitivity over chopped CW illumination and synchronous detection. A simple sensitivity estimate based on an assumed range of 8 m, a 30 Hz frame rate, a primary collection area of 30 cm diameter, and an overall optical efficiency of 50 %, yields a noise-equivalent reflectance difference of 0.66 % in a single frame. The uncooled niobium microbolometers provide a (measured) noise-equivalent power of 100 $pW/Hz^{1/2}$ and a time constant of 175 ns, well matched to the source pulse width and the system sensitivity requirements. Optical coupling is provided by resonant slot-ring antennas, distributed in a focal plane array covering a single 75 mm diameter wafer. The optical and electrical systems used for coupling signals into and out of the focal plane array are also described.

Keywords: Bolometer, array, millimeter-wave, concealed weapons, imaging

1. INTRODUCTION

This paper describes the detailed design of an active millimeter-wave imaging system for the detection of weapons concealed on the human body beneath clothing. The high transparency of clothing at millimeter wavelengths and the spatial resolution required to form adequate images of concealed weapons combine to make imaging at millimeter wavelengths a natural approach for this application. Because of the importance and market size associated with this application, a number of previous programs have explored device performance, and even developed complete prototype systems of this kind[1-4]. The chief technical challenges identified in previous work have been (a) raw sensitivity, and (b), in narrow bandwidth systems, glint arising from uncontrolled standing waves generated between the target and its environment. A more detailed comparison of the various technical strategies available for concealed weapons detection is provided in a companion paper at this conference[5]. In general however, passive systems tend to suffer most in the area of sensitivity, while active systems tend to be more limited by glint and other systematic uncertainties in the final images. Although technical means exist to overcome both these issues (using cryogenic focal plane arrays, for example, to improve sensitivity), the ability to obtain adequate images at adequate speed in a system that could be manufactured at low cost has yet to be demonstrated. As described more fully in the companion paper, "adequate" for this application means that, at a range of 5 – 8 m, recognizable images of concealed weapons can be produced at a standard 30 Hz video frame rate. A spatial resolution on the target of ~ 1 cm is adequate to produce such images. The field-of-view must cover an entire human form – maximum diameter of 2m – at the above range. However, the maximum field-of-view and and maximum spatial resolution do not have to be obtained simultaneously. (Indeed, this would require a much larger format array than that described here.) The overall system package is envisioned to comprise something that could be mounted on a vehicle that is driven into a crowd, and then scanned to identify those individuals bearing concealed weapons.

The approach taken in this work is to combine the chief advantages of both active and passive systems. The system is active, illuminating the target with a strong mm-wave source and detecting the reflected radiation. This raises the power levels to be detected by many orders of magnidtude over a passive imaging system,and enables the use of simple, uncooled, antenna-coupled bolometers as the detecting elements. On the other hand, it is a relatively broadband system (5 % fractional bandwidth), which eliminates the possibility of glint. Such an architecture requires a high power mm-wave source with large instantaneous bandwidth. For this we use high power Si IMPATT (impact ionization avalanche transit-time) oscillators, which operate at 95 (± 2.5) GHz in pulsed mode. Their maximum peak power and duty cycle are approximately 1 W and 1

---

[*] Contribution of the U. S. Government, not subject to copyright

[**] grossman@boulder.nist.gov; (303) 497-5102; fax (303) 497-3042

% respectively, limited by thermal dissipation. They are commercially available, at low enough cost to avoid prohibitive impact on overall system cost.

The main focus of this paper however, is the detection system, centered on a focal plane array (FPA) of uncooled, mm-wave bolometers. The FPA consists of a 75 mm diameter Si wafer, populated by a 117-element array of thin-film Nb bolometers, each of which is coupled to the incident radiation by a planar, lithographically fabricated, mm-wave antenna. Each microbolometer's output feeds a separate channel of fast analog pre-amplification and gated integration, located off wafer. No multiplexing or digitization is performed until after the signal bandwidth is greatly reduced by coaddition of several thousand pulses. This paper is organized as follows: we first describe a rough estimate of the system sensitivity, adequate to demonstrate the feasibility of the pulsed-system concept and to illustrate the system's advantage over a system based on CW illumination. We then describe the Nb microbolometer that forms the core of each unit cell in the FPA, focussing on a recent improvement we have made to the single-pixel performance through use of a new fabrication process. The following section describes the layout of the array, concentrating on the rationale behind the particular layout and wiring scheme selected. It also describes the design for electrical bias and readout of the array, which has been somewhat modified from the configuration used in our single-pixel experiments in order to ease the on-wafer wiring requirements. The next section describes the present status of the optical design of the system. In the last section, we summarize the present status of the system demonstration and outline the near-term plans for the program.

2. SENSITIVITY ESTIMATE

Since this system operates on the principal of imaging contrasts in reflectance of the target, it is natural to analyze its sensitivity in terms of a noise-equivalent reflectance difference (NERD), analogous to the noise-equivalent temperature difference (NETD) commonly used to characterize IR imaging systems. It is specified on a per-pixel basis; coadditon of pixels results in improved measurement of reflectance contrast (lower NERD), at the expense of spatial resolution. We define the NERD to be simply the reflectance contrast that can be detected between two pixels, with unity signal-to-noise ratio, when the mean reflectance is given by isotropic scattering of the illuminating radiation into the backward hemisphere. The reflected radiation is collected by an optical system, whose entrance aperture (i.e. the primary mirror) is defined to have diameter D, while L is the range to the target. The output of the pulsed mm-wave source will be described as a peak power P that remains constant during the pulse duration τ_p, is zero at other times during the cycle, and is periodic at the repetition rate f_r. The mm-wave source is focussed in such a way as to illuminate the field imaged by the N_{pix}-element FPA. For example, when imaging the full 2 m diameter field at a range of 8 m, the mm-wave source must fill a 7° halfwidth beam, which corresponds fairly closely with the corrugated feedhorn output used in our single-pixel antenna coupling experiments[6]. Ideally, the mm-wave power would be distributed over the N_{pix}-element field uniformly, with zero power distributed outside this field, but for a realistic sensitivity analysis, we assign an efficiency ε_s of order 50 %, to this power distribution problem. In this case, the peak power received at each pixel is given by

$$P_{pp} = P\frac{\varepsilon_s R}{N_{pix}}\left(\frac{D^2}{8L^2}\right), \tag{1}$$

where R is the total hemispherical reflectance of the target. For the typical values listed in Table 1, this comes to 0.37 μW. The fundamental quantity for discussing sensitivity in this case is the RMS uncertainty in the reflected power measurement, σ_p. If this is limited by detector sensitivity, then it is given by

$$\sigma_p = \frac{NEP}{(2\tau)^{1/2}}, \tag{2}$$

where the noise-equivalent power, NEP, is the usual figure of merit describing detector sensitivity, and τ is the integration time of the measurement. When $\tau = \tau_g$, the gate width, then (2) describes the uncertainty on a per-pulse basis. In a power measurement based on periodic gated integration (i.e. a conventional "boxcar" integration configuration), (2) applies with $\tau = N_g \tau_g$, where N_g is the number of gated pulses whose outputs are averaged. The number of pulses averaged is simply the ratio of the pulse repetition rate to the frame rate, $N_g = f_r / f_f$, and is typically ~ 3000 for our system. (Note that (2) assumes the detector noise is frequency independent over the relevant frequency range, which will be discussed further below.) If σ_p is limited by detector sensitivity, then the quality of the reflected image is best described by the NERD,

$$P_{pp} = P \frac{\varepsilon_s R}{N_{pix}} \left(\frac{D^2}{8L^2} \right) \quad . \tag{3}$$

For the typical system parameters given in Table 1, we obtain NERD = 0.66 % in a single frame, with a 30 Hz frame rate. This sensitivity level is more than adequate for detection and imaging of most concealed weapons. Metallic objects will produce reflectances R ~ 100 %, 50 % greater than the assumed mean R, and therefore a 1 σ signal-to-noise ratio of ΔR/NERD = 75. Even many non-metallic objects should yield easily detectable reflectance differences with this level of NERD.

Frame Rate	f_f	30 Hz
Repetition Rate	f_r	100 kHz
Peak Source Power	P_{sp}	1 W
Average Source Power	P_{sa}	10 mW
Pulse Width	τ_p	100 ns
Gate Width	τ_g	250 ns
Detector Time Constant	τ_d	175 ns
Detector Optical NEP	NEP	100 $pW/Hz^{1/2}$
Detector Electrical NEP	NEP_e	50 $pW/Hz^{1/2}$
Range	R	8 m
Primary Mirror Diameter	D	30 cm
Number of pixels	N_{px}	120
Source Optical Efficiency	ε_s	50 %
Target Mean Absorptance	A	50 %
Target Mean Reflectance	R	50 %, uniform over 2π sr solid angle

Table 1. Typical system parameters, as used in the sensitivity calculation described in the text.

As discussed at greater length by Nolen et al.[7], comparison of the above sensitivity with that of an active system based on CW illumination and synchronous detection should be made under the assumption of equal *average* powers in the pulsed and CW sources. In this case, the signal-to-noise ratio for measurement of reflectance differences is superior for the pulsed system, by a factor of the square root of the duty cycle, i.e. by a factor of 10 for our parameters.

3. SINGLE-PIXEL MICROBOLOMETER PROPERTIES

The bolometers used here have been described in detail in previous publications[7,8]. They consist of 20 nm thick films of Nb, deposited by DC magnetron sputtering and patterned by conventional optical lithography into 2 μm × 6 μm (width × length) active elements. Thermal isolation is provided by an unpatterned layer of thermally grown SiO_2, approximately 2 μm thick, lying between the Nb and the Si substrate. The 150 nm thick Au antenna layer is deposited in a subsequent deposition step, after cleaning the Nb surface in a low power Ar plasma. At room temperature, the bolometers' temperature coefficient of resistance $(R^{-1})\, dR/dT$ is typically 0.2 % K^{-1}, not too far from the ideal normal metallic value of 1/T. Thermal isolation typically lies in the range of G = 20 – 50 μW / K, yielding specific responsivity of 2 – 5 V / W-mA. The maximum electrical responsivity is limited by the maximum bias current. Ordinarily the measured resistance varies with bias in accordance with the standard self-heating model of a lumped bolometer, i.e. $V/I = R_0 + (dR/dT)\, \Delta T$, $VI = G\, \Delta T$, up to a certain limit in current. (Here R_0 is the bolometer's zero-bias resistance and $\Delta T = T - T_{amb}$ the elevation in its temperature above ambient, at the operating point.) This limit is manifested in a plot of differential resistance versus bias current as a peak occurring at some high bias I_{peak}, which lies well below the current at which the standard self-heating model would predict a divergence in dV/dI, namely $I_{\max} = \left(G^{-1} \frac{dR}{dT} \right)^{-1/2}$. At currents somewhat below I_{peak} the measured optical responsivity stops increasing with bias, while at or slightly above I_{peak}, the bolometer's I-V characteristic changes irreversibly. Because the value of I_{peak} can vary dramatically depending on the in-situ cleaning procedure applied to the Nb surface prior to Au deposition, we have always attributed the above behavior to parasitic contact resistance at the Nb/Au interface. Moreover, in an extensive set of recent measurements, we observed the value of I_{peak} to decrease monotonically with increasing ambient temperature, consistent with $VI_{peak} \propto T_{\max} - T_{amb}$. This tends to confirm the suspicion that ohmic dissipation at the contact heats the interface, enabling some type of thermally activated process to degrade the bolometer responsivity, and eventually the device integrity.

More recently, we have developed (under a different program) a new fabrication process for the Nb/Au antenna-coupled bolometers, based on blanket deposition of a Nb/Au bilayer without breaking vacuum. Definition of the bolometer is accomplished by a selective etch step which removes the Au but stops without etching through the thin Nb. As shown in Fig. 1, this has yielded a dramatic increase in I_{peak}, by approximately a factor of 4. This enables the bolometers to be run at higher bias, with correspondingly higher responsivity. Typical values for the responsivity will improve from $\Re$ = 10 V/W (3 mA bias at 3.3 V/W-mA) to $\Re$ = 40 V/W. As the bolometer sensitivity is limited by a roughly equal combination of amplifier and Johnson noise to $NEP = \frac{1.5nV / Hz^{1/2}}{\Re}$, this will provide electrical NEP < 35 pW/Hz$^{1/2}$, well below the design specification (Table 1.). This will provide additional margin on the optical efficiency specification.

It is important to realize that the noise properties of the Nb bolometers make a pulsed system much better suited to their use than a CW architecture. This is simply because the frequency of the knee in the 1/f-noise spectrum typically lies in the range of 1 kHz[8]. This is far below the repetition rate for our pulsed architecture, and therefore 1/f noise does not contribute to the uncertainty in reflected pulse power. In a CW system, this condition would be difficult to achieve, because easily implemented modulation schemes for most CW mm-wave sources would be limited to kHz frequencies or below.

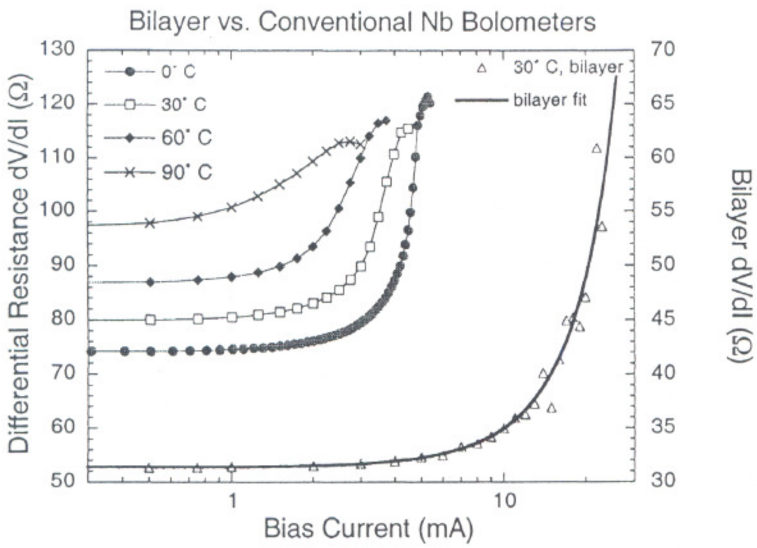

Fig. 1. Electrical responsivity characteristics of a conventionally fabricated Nb bolometer, at several ambient temperatures, compared with that of a bolometer fabricated from an in-situ Nb-Au bilayer.

4. ARRAY LAYOUT AND READOUT

The bolometers in this FPA are coupled to the incident radiation through cavity-backed, slot-ring antennas. This antenna design was selected because of its simplicity of fabrication (no insulation layers required for microstrip components), polarization flexibility, and ease of arraying. The fact that a large-format array is to be constructed implies that no substrate lenses or other mechanically assembled (i.e. non-monolithic) 3-dimensional structures can be used. In this case, the problem of substrate modes prevents the use of electrically thick substrates[9,10]. An electrically thin substrate is quite feasible however, even without the use of micromachined membranes ($\frac{\lambda_0}{20\sqrt{\varepsilon}} = 50\ \mu m$ in Si, and is the substrate thickness used for the FPA). The purpose of the backing cavity, which is simply a reflecting plane located an odd number of quarter-wavelengths behind the FPA, is simply to recover the 3 dB of response that would otherwise be lost to coupling to the backside of the antenna. Slot-ring antennas in free space and on electrically thick substrates have been well studied in recent years[11-13], but their implementation with a backing cavity of this type is novel. We have performed detailed analytic, numerical, and experimental studies of this configuration, both in single pixels and 5-element arrays, which are described at length in a companion paper at this conference[6]. These studies have yielded the necessary design values of slot diameter, slot width, antenna spacing and cavity length. In contrast to previous slot-ring antenna designs, the groundplane is truncated at an outer diameter approximately twice that of the ring. The truncation of the groundplane, which is necessary in order to realize the directivity and coupling improvements afforded by the backing cavity, modifies the resonant frequency. However, the modification is only slight, from 95 GHz to 91 GHz. The antennas in the prototype 117-element array are therefore identical to those in the single-element and 5-element antenna studies. The impedance at 95 GHz, according to the numerical model, is $115 - j50\ \Omega$. This can be well matched to the Nb bolometer resistance, which is given simply by the Nb surface resistance of ~ 25 Ω/square. Therefore, for the large array, the bolometer size is increased from 2×6 μm to 2×10 μm to improve the impedance match. Although the wiring lengths on the 117-element array are relatively large, parasitic wiring resistance can be kept below < 50 Ω, by increasing the thickness of Au deposited.

The strategy for laying out the 117-element array is illustrated in Fig. 2. The antennas are arranged on an 11 x 11 square grid with the 4 corner elements removed. The grid pitch is 4.75 mm, determined on the basis of the 5-element array studies. The trade-off is simply between lower pixel count and reduced spatial resolution, which occur for too sparse an array, and electromagnetic interaction between the antennas, (reducing the coupling efficiency and increasing the crosstalk), which occurs for too dense an array. The results from the 5-element arrays bracketed the optimum value for array pitch between 5 and 2.5 mm; thus, the 4.75 mm value chosen is likely to err somewhat on the sparse side. The issue of electromagnetic interaction also dominates the question of locating the wires for DC bias and readout of the individual pixels. The strategy used for resolving this issue is to orient all wires within a pixel normal to the E-plane of that pixel's antenna. Moreover, all wire widths are much less than a dielectric wavelength. In this way, any currents excited on the wiring by the incident co-polarized radiation will be confined to lengths << wavelength, and therefore the efficiency for absorbing or scattering radiation by these currents should be very much lower than that of the antenna. In order to physically accommodate this strategy, the grid on which the antennas are arranged is rotated by 8 degrees from the orientation of the wiring. This angle allows the wires from each antenna to pass beside, rather than, through the neigboring antennas. Contact pads for connection to off-wafer electronics are placed on the four sides of the array. Electrical contact is made through commercial, metallized elastomeric connectors to four "flex" circuitboards which host the front-end electronics. Physical support is also provided by the metallized elastomeric connectors, which have enough mechanical compliance to effectively insulate the wafer from mechanical shock and vibration.

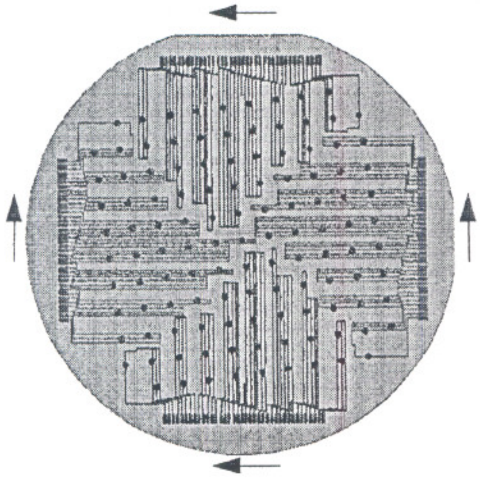

Fig. 2. Layout of the prototype 117-element uncooled, antenna-coupled bolometer array. Arrows indicate the alternating polarization sensitivity of the four quadrants. The wafer diameter is 75 mm.

The strategy for electrical bias and readout of the 117-element array is illustrated in Fig. 3. The bolometers are voltage-biased in parallel, and their currents read out through individual transimpedance amplifiers. In the single-pixel experiments on the other hand, we have generally biased the bolometers from a current source and read out the signal though a differential voltage amplifier. In most cases, the bolometers have been tested in a 4-terminal configuration to enable accurate resistance measurements in the presence of significant parasitic resistance from on-chip wiring. In the case of the 117-element array, two considerations argue for the alternative approach illustrated in Fig. 3. First, because in the usual failure mode the bolometers become open rather than short circuits, a parallel bias for a large array is much more fault tolerant. Voltage bias then ensures that the bias point of each bolometer remains independent of the resistance of the other bolometers. Second, transimpedance readout of bolometer current requires only one wire per element to connect to the external electronics, because the voltage bias is parallelized on-wafer. Parasitic wiring resistance only affects the array by adding an offset to the voltage bias of each bolometer; as long as the wiring resistance and therefore the offset are approximately equal for all the pixels, the wiring resistance should have no effect on performance. As can be seen in Fig. 3, the wiring layout is designed to equalize as much as possible the parasitic wiring resistances of all pixels.

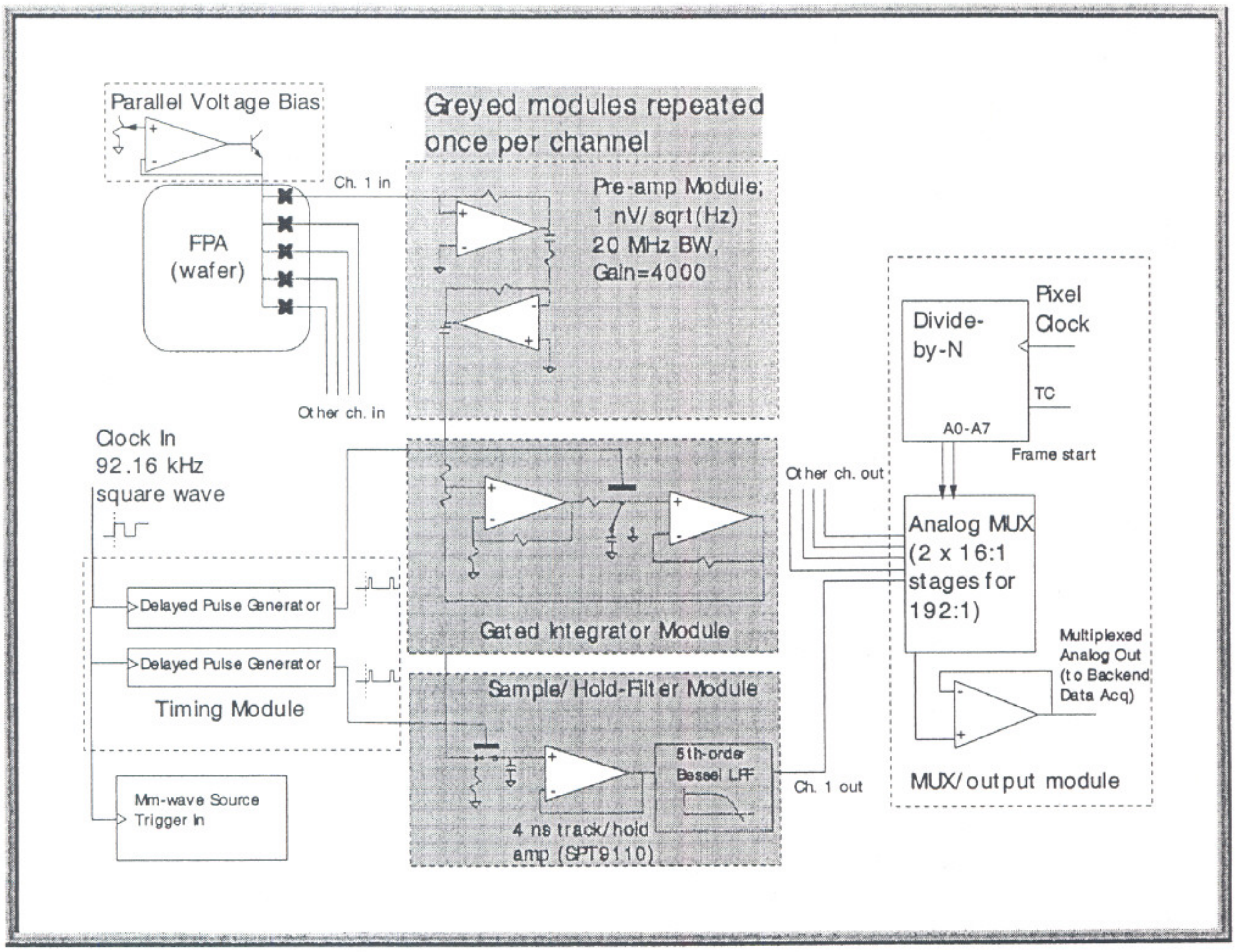

Fig. 3. Block diagram of the bias and readout electronics for the 117-element array.

The electronics which follow the transimpedance amplifier are also illustrated in Fig. 3. The gain of the AC-coupled amplifier stages is set by requiring a dynamic range of 100, defined in this case as the ratio of the amplitude of the largest pulse which can be measured without saturation, to the RMS noise within the (20 MHz) preamp bandwidth. This value of 100 defines the resolution in the greyscale of the final image. The pre-amplifier is followed by a gated integrator module.

The gate width is determined by a straightforward calculation: for an input pulse consisting of an exponential rise, of duration τ_{100}, with time constant τ_b, followed by an exponential fall, also with time constant τ_b, what is the gate width which optimizes signal-to-noise ratio in a measurement of the integrated pulse amplitude ? The values of τ_{100} and τ_b, the width of the radiated mm-wave pulse, and the bolometer time constant respectively, are approximately 100 and 175 ns, as determined by direct measurement in earlier single-channel experiments[7]. The result, for these particular values, is τ_{opt} = 300 ns, and the signal-to-noise ratio degrades relatively slowly when the gate width deviates from the optimum. Following the gated integrator is a fast sample-and-hold amplifier and low-pass filter, to convert the train of integrated pulse heights to a DC level proportional to the average pulse height within the time period defined by the low pass filter. This latter time period is simply the frame period $1/f_r$ = 33 ms. The output module is simply an analog multiplexer and buffer to pass the array output (the N_{pix} DC levels) to a backend data acquisition and display module housed in a laptop computer[5].

5. ARRAY OPTICS

The optical design is based on a dual-configuration concept, exploiting the fact that maximum spatial resolution is not required simultaneously with maximum field-of-view. In one configuration, which we describe as "widefield", the system will image the entire 2 m diameter field of the target. Given the fixed 75 mm diameter of the focal plane, this implies a system magnification of m_{wide} = 0.038. The other configuration, termed "narrowfield", is intended to provide a zoomed-in image of a selected region of the target, at maximum spatial resolution. A value of m_{narrow} = 0.5 was selected for the magnification of this configuration, as an initial guess for the optimal tradeoff between spatial resolution (which improves with larger magnification) and off-axis coupling efficiency, which improves at lower magnification, due to reduced aberrations. The physical design of the optics is intended to allow rapid switching between the two configurations. In particular, the two configurations are required to employ the same primary mirror. The secondary mirrors are mounted on a rotatable wheel.

The overall procedure for the optical design is to begin with a rough, on-axis design based on intuition and the minimization of geometric, 3rd-order aberrations. This is essentially a Cassegrain telescope, adapted for a finite object distance. This design is then used as the starting point for iterative refinements, using a commercial physical optics code that includes diffraction. In the course of this refinement, the design can be modified to an off-axis configuration by defining an off-axis entrance pupil. This procedure is not yet completed, but it nonetheless is worthwhile to describe the current status of the design, because it likely does indicate roughly the capabilities and main issues with the final optical system.

The design procedure begins with the analytic formulae describing a 2-mirror system that is aplanatic to 3rd order[14]§8, i.e. in which the 3rd order spherical aberration and coma are both zero. In such a 3rd order design, both primary and secondary mirrors are conic sections. Such a system is parameterized by five independent quantities, though a variety of choices may be made for which quantities these are. In this case, we use the primary and secondary magnifications, the paraxial ray-height ratio Ω, the object distance, and the entrance pupil distance. Because the primary mirror itself forms the entrance pupil for the system, the latter two quantities are both fixed at the value of 8 m, given by the overall system specifications. Then, for each fixed system magnification, corresponding to the widefield or narrowfield configuration, a 2-d matrix of solutions is generated, parameterized by the primary magnification m_1, and the paraxial ray-height ratio. It turns out that under these requirements, the system is overconstrained. There is no pair of aplanatic solutions – widefield and narrowfield - which share a common primary. The aplanatic solutions for the widefield configuration have primaries which are either hyperboloids or oblate ellipsoids (depending on the sign of Ω), while aplanatic solutions for the narrowfield configuration all require prolate ellipsoidal primaries. Therefore, the following strategy is used. The widefield configuration places more stringent requirements on the design because a higher curvature secondary is required, and aberrations increase with increasing curvature. Therefore, for the widefield design, we select a 3rd order solution which is not only aplanatic, but which also has zero 3rd order astigmatism. This leads to a paraxial ray-height ratio of ~ 0.23, which is reasonable in terms of obscuration of the primary (obscured fraction is simply Ω^2.) For the narrowfield design, the same primary is used, while the secondary's curvature is selected to produce the correct system magnification, and the secondary's conic constant selected to eliminate 3rd order spherical aberration.

At this point the 3rd order geometric design is used as a starting point for full physical optics calculations. The procedure is to optimize the widefield design by first adding higher-order corrections to the shape of the widefield secondary, then adding higher-order corrections to the shape of the primary. Finally, holding the primary fixed, the narrowfield design is optimized by adding higher-order corrections to the shape of the narrowfield secondary. As a benchmark calculation for quantitatively evaluating an optical design, we use the following: an array of point sources is defined in the object plane (i.e. on the target).

It consists of two linear arrays, one along the horizontal and vertical axes of the image. They extend from the center of the field out to the edge of the wide or narrow field, respectively. The spacing of the array elements is adjusted to approximate the pixel spacing in the FPA, divided by the system magnification. The point sources thus represent adjacent resolution elements on the target. Radiation from these point sources is propagated through the optics to the FPA. To the extent that the radiation from adjacent sources overlaps in the focal plane, the optical system can degrade the spatial resolution of the system. To the extent that the radiation from sources at the edge of the field is reduced in amplitude in the focal plane, optical aberrations can restrict the field-of-view of the system, by decreasing the optical coupling efficiency at the edge of the image. Fig. 4 shows an example of this, for the widefield configuration, which is the more demanding of the two. The shaded region represents the 75 mm diameter wafer within the FPA. The outermost elements of the FPA (see Fig. 2) lie at a radius of 28 mm, to allow clearance for the wiring and connectors at the edge. In the left panel, the point sources on the target are spaced by 15 cm, and the images in the focal planes are clearly well resolved. In the right panel, the sources on the target are spaced by by 12.5 cm, and the images are poorly resolved. The latter spacing on the target corresponds exactly to the pixel spacing in the focal plane. Thus, the spatial resolution of the FPA is clearly degraded somewhat by the optics. Moreover, the peak intensities at the edge of the field are reduced, by approximately a factor of 4, compared to the center. On the other hand, the optical design whose performance is illustrated in Fig. 4 only incorporates 4th order corrections to the shape of the secondary; there is considerable scope for further optimization.

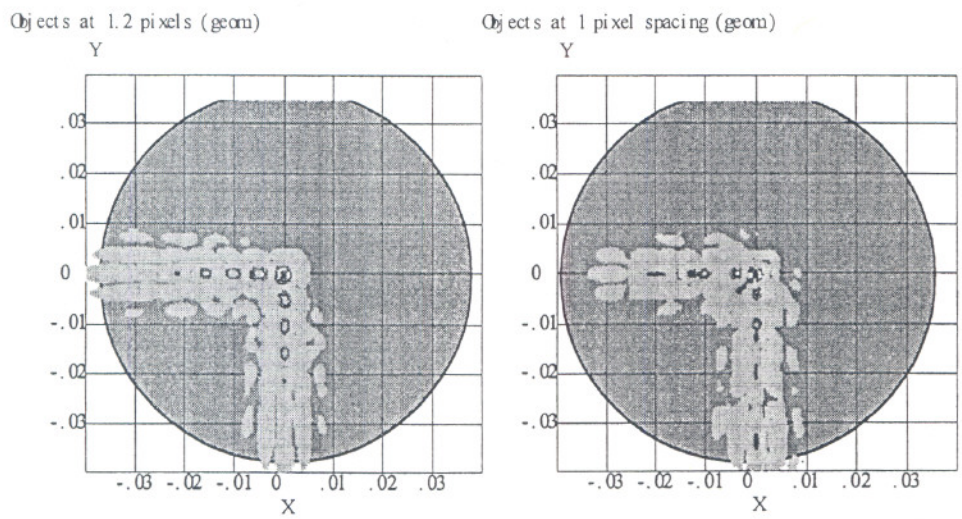

Figure 4. Calculated power density delivered to the focal plane by the on-axis, modified Cassegrain design in the "widefield" configuration described above (see Fig. 2), for two different source distributions. One the left, the source distribution consists of two linear arrays of points separated by 1.2 times the pixel separation, while on the right, the source separation corresponds to the pixel separation.

6. SUMMARY AND PRESENT STATUS

The detailed design of a 117-element focal plane array of uncooled, antenna-coupled bolometers has been described. Detailed measurements of the sensitivity and radiation patterns of single pixels and 5-element arrays have been completed. Significant changes to the design of the large array are being made in three areas. First, the parasitic contact resistance can be greatly reduced with a modified bolometer fabrication process. This will provide a factor of >4 improvement in NEP, and has been demonstrated on a single pixel. Second, the bias and first-stage of readout electronics will be modified, from a current bias with differential amplifier readout, to a parallel voltage bias with transimpedance amplifier readout. This will reduce the per-pixel wire count from four to one, and provide a much higher measure of fault tolerance to the failure of individual pixels. Design is complete on this modification, but fabrication and test of the electronics is currently underway. Finally, optical coupling to the FPA requires careful design, which is presently underway, in order to maintain high coupling efficiency out to the edge of the array and to preserve the spatial resolution available from the FPA. In the present, non-optimized design, the optical system is the limiting component for the system spatial resolution.

7. ACKNOWLEDGEMENTS

We are very grateful to D. Bergmann for the design and assembly of the backend data acquisition system. We are also grateful to the National Institute of Justice and the Federal Aviation Adminisitration, which have provided financial support for this program, through the NIST Office of Law Enforcement Standards.

8. REFERENCES

[1] G. R. Huguenin, "Millimeter Wave Concealed Weapon Detection and Through-the-Wall Imaging Systems",*Proc. SPIE* **2938,** pp. 152-159, (1997).

[2] J. A. Lovberg, J. A. Galliano, and S. E. Clark, "Passive Millimeter-wave Imaging for Cocealed Article Detection",*Proc. SPIE* **2938,** pp. 120-130, (1997).

[3] Y.-W. Chang, M. Juhola, and W. Grainger, "Millimeter-wave Concealed Weapon Detection",*Proc. SPIE* **2938,** pp. 131-138, (1997).

[4] D. L. McMakin, D. M. Sheen, T. E. Hall, and R. H. Severtsen, "Cylindrical Holographic Radar Camera",*Proc. of the SPIE* **3575,** pp. 79-88, (1998).

[5] N. G. Paulter, E. N. Grossman, G. N. Stenbaken, B. C. Waltrip, S. Nolen, and C. D. Reintsema, "Design of an Active Mm-wave Concealed Object Imaging System",*Proc. SPIE* **4373,** pp. , (2001).

[6] S. Nolen, T. E. Harvey, C. D. Reintsema, and E. N. Grossman, "Slot-ring Antennas with a Planar backshort Designed for Millimeter-Wave Applications",*Proc. SPIE* **4373,** pp. , (2001).

[7] S. Nolen, J. A. Koch, N. G. Paulter, C. D. Reintsema, and E. N. Grossman, "Antenna-coupled Niobium Microbolometers for Millimeter-wave Imaging Arrays",*Proc. SPIE* **3795,** pp. 279-286, (1999).

[8] M. E. MacDonald, Grossman, E. N., "Niobium Microbolometers for Far-infrared Detection",*IEEE Trans. on Microwave Theory and Techniques* **43,** pp. 893-896, (1995).

[9] N. G. Alexopoulos, P. B. Katehi, and D. B. Rutledge, "Substrate Optimization for Integrated Citcuit Antennas",*IEEE trans. Microwave. Theory and Tech.* **MTT-31,** pp. 550-557, (1983).

[10] G. M. Rebeiz, "Millimeter-Wave and Terahertz Integrated-Circuit Antennas",*Proc. of the IEEE* **80,** pp. 1748-1760, (1992).

[11] C. E. Tong and R. Blundell, "An Annular Slot Antenna on a Dielectric Half-Space",*IEEE Trans. Antennas and Propagation* **42,** pp. 967-974, (1994).

[12] N. Nikolic, "Theoretical and Experimental Study of a Cavity-backed Annular-Slot Antenna",*IEE Proc.-Microwave Antennas and Propagation* **144,** pp. 337-340, (1997).

[13] S. Raman and G. M. Rebeiz, "Single-and Dual-Polarized Millimeter-wave Slot-ring Antennas",*IEEE Trans. Ant. and Prop.* **44,** pp. 1438-1444, (1996).

[14] D. Korsch, *Reflective Optics*, 1st ed. (Academic Press, San Diego, 1991).

Passive Millimeter-Wave Imaging Technology V

Roger M. Smith
Roger Appleby
Chairs/Editors

19 April 2001
Orlando, USA

Sponsored and Published by
SPIE—The International Society for Optical Engineering

The papers appearing in this book compose the proceedings of the technical conference cited on the cover and title page of this volume. They reflect the authors' opinions and are published as presented, in the interests of timely dissemination. Their inclusion in this publication does not necessarily constitute endorsement by the editors or by SPIE. Papers were selected by the conference program committee to be presented in oral or poster format, and were subject to review by volume editors or program committees.

Please use the following format to cite material from this book:

Author(s), "Title of paper," in *Passive Millimeter-Wave Imaging Technology V*, Roger M. Smith, Roger Appleby, Editors, Proceedings of SPIE Vol. 4373, page numbers (2001).

ISSN 0277-786X
ISBN 0-8194-4068-X

Published by
SPIE—The International Society for Optical Engineering
P.O. Box 10, Bellingham, Washington 98227-0010 USA
Telephone 1 360/676-3290 (Pacific Time) • Fax 1 360/647-1445
http://www.spie.org/

Printed in the United States of America.